


Hyperresponsiveness of mice deficient in plasma-secreted sphingomyelinase reveals its pivotal role in early phase of host response

Nayla Jbeily,^{*,†} Iris Suckert,^{*} Falk A. Gonnert,^{*} Benedikt Acht,^{*} Clemens L. Bockmeyer,[§] Sascha D. Grossmann,^{*} Markus F. Blaess,^{*} Anja Lueth,^{**} Hans-Peter Deigner,^{††} Michael Bauer,^{*} and Ralf A. Claus^{1,*}

Center of Sepsis Control and Care,^{*} Jena University Hospital, Jena, Germany; International Leibniz Research School,[†] Jena, Germany; Institute for Pathology,[§] Hannover Medical School MHH, Hannover, Germany; Department of Nutritional Toxicology,^{**} Institute of Nutritional Science, University of Potsdam, Potsdam, Germany; and University of Applied Science Furtwangen,^{††} Furtwangen, Germany

Abstract Plasma secretion of acid sphingomyelinase is a hallmark of cellular stress response resulting in the formation of membrane embedded ceramide-enriched lipid rafts and the reorganization of receptor complexes. Consistently, decompartmentalization of ceramide formation from inert sphingomyelin has been associated with signaling events and regulation of the cellular phenotype. Herein, we addressed the question of whether the secretion of acid sphingomyelinase is involved in host response during sepsis. We found an exaggerated clinical course in mice genetically deficient in acid sphingomyelinase characterized by an increased bacterial burden, an increased phagocytotic activity, and a more pronounced cytokine storm. Moreover, on a functional level, leukocyte-endothelial interaction was found diminished in sphingomyelinase-deficient animals corresponding to a distinct leukocytes' phenotype with respect to rolling and sticking as well as expression of cellular surface proteins.  We conclude that hydrolysis of membrane-embedded sphingomyelin, triggered by circulating sphingomyelinase, plays a pivotal role in the first line of defense against invading microorganisms. This function might be essential during the early phase of infection leading to an adaptive response of remote cells and tissues.—Jbeily, N., I. Suckert, F. A. Gonnert, B. Acht, C. L. Bockmeyer, S. D. Grossmann, M. F. Blaess, A. Lueth, H.-P. Deigner, M. Bauer, and R. A. Claus. **Hyperresponsiveness of mice deficient in plasma-secreted sphingomyelinase reveals its pivotal role in early phase of host response.** *J. Lipid Res.* 2013. 54: 410–424.

Supplementary key words sphingomyelin phosphodiesterase 1 • inflammation • sepsis • gene expression • survival • leukocyte-endothelial interaction • trans-migration • organ failure

Sepsis is defined as a syndrome with a complex continuum of host responses to invading microorganisms. These pathophysiological changes affect more than 1.5 million patients in Europe alone. Similarly, 20% of patients admitted to intensive care units (ICUs) in the United States suffer from severe sepsis, which is the leading cause of mortality in noncardiac ICUs. Despite the development of early intervention and intensive care, mortality resulting from sepsis is unacceptably high, reaching 30 to 50% in hospitals worldwide (1–3). The host response to infection is mediated by pathogen components (e.g., lipopolysaccharides or zymosan) and by host-activated enzymes, mediators (such as proinflammatory cytokines), and cells changing their phenotype. The resulting remote organ failure is associated with a poor outcome.

Generation of the lipid mediator ceramide has been suggested as one major route of cellular response to stress (4). Activation of ceramide-generating enzymes that hydrolyze cell membrane embedded sphingomyelin is implicated in mediating and regulating diverse cellular processes, such as proliferation, differentiation, apoptosis, and inflammation (5, 6). Moreover, ceramide formation is involved in the pathogenesis of numerous diseases, such as cancer, atherosclerosis, pulmonary edema, and cardiovascular disease

This work was supported by the Deutsche Forschungsgemeinschaft (R.A.C. as a member of SPP 1267: Sphingolipids - Signal and Disease), by the Hans-Knoell-Institute (Jena, Germany) and the International Leibniz Research School for Microbial and Biomolecular Interactions Jena as part of the excellence graduate school Jena School for Microbial Communication (N.J.), and by the Center for Sepsis Control and Care.

*Author's Choice—Final version full access.

Manuscript received 29 August 2012 and in revised form 10 December 2012

Published, JLR Papers in Press, December 10, 2012

DOI 10.1194/jlr.M031625

Abbreviations: ALT, alanine transaminase; aSMase, acid sphingomyelinase; AST, aspartate transaminase; BW, body weight; CFU, colony-forming unit; GGT, gamma glutamyl-transferase; ICU, intensive care unit; IL, interleukin; MFI, mean fluorescence intensity; MCP, monocyte chemotactic protein; PCI, peritoneal contamination and infection; T-Bil, total bilirubin; TNF, tumor necrosis factor.

¹To whom correspondence should be addressed.

e-mail: ralf.claus@med.uni-jena.de

(7–10). Five isoforms of specific, sphingomyelin hydrolyzing phosphodiesterases or sphingomyelinases have been identified (11, 12).

The secreted acid sphingomyelinase (aSMase) is the only isoform associated with extracellular hydrolysis of sphingomyelin and has been found to be secreted by macrophages, human skin fibroblasts, and human vascular endothelial cells (13, 14). Apical secretion by endothelial cells was stimulated by a variety of proinflammatory mediators and cytokines, such as tumor necrosis factor (TNF)- α , interleukin (IL)-6, IFN- β , or IL-1 β , but also by membrane constituents of gram-negative bacteria (14). It was previously shown that patients with chronic or acute systemic inflammation or infection such as sepsis exhibited an enhanced sphingolytic activity in comparison to controls (15, 16). During progression of the disease, a further increase in the activity of secreted aSMase parallel to severity of illness predicts a fatal outcome (15). Furthermore, in mononuclear cells of septic patients, the concentration of ceramide was increased and correlated positively with plasma TNF- α levels and was higher among patients who developed dysfunction of remote organs (17, 18). A 2- to 3-fold rise in plasma sphingolytic activity was also observed in animal models after application of endotoxin or proinflammatory cytokines (15, 19). As the inert membrane constituent, sphingomyelin is preferentially distributed in the outer leaflet of cellular membranes. After inflammation-triggered secretion, aSMase gains unlimited access to its substrate and produces huge amounts of ceramide, affecting membrane organization (20, 21). In an instantaneous manner, ceramide induced the release of reactive oxygen species in endothelial cells, decreasing endothelium-dependent vasorelaxation (22, 23). These observations support the concept that secreted aSMase is a key player in cytokine secretion during host response. This sequence of cellular response to inflammatory stress also put forward the hypothesis that an unfavorable outcome of sepsis-associated remote organ failure might be linked to regulating the secretion and activation of aSMase.

MATERIALS AND METHODS

Animals

Transgenic mice with a deficiency in aSMase function (knock-out [KO]) (aged 8–10 weeks) and their wild-type (WT) littermates (aged 8–12 weeks) were used in this study (24). Animals were randomly selected for each experiment, were maintained under artificial day-night conditions at room temperature, and received a standard diet and water ad libitum. All experiments were performed in accordance with the German legislation on protection of animals and with permission of the regional animal welfare committee. Mice were anesthetized with a combination of ketamine and xylazine injected intraperitoneally before any surgical procedure. During the surgical procedures, body temperature was maintained at 37°C.

Sepsis model

Sepsis was induced using the peritoneal contamination and infection (PCI) model as previously described (25). In the present study, peritonitis was induced by the injection of a 1:4 diluted

stool suspension (5 μ l/g body weight [BW]) intraperitoneally. Two postinsult time points were selected to represent early sepsis (6 h) and late sepsis (18–24 h).

Survival analysis

For survival analysis, aSMase WT and KO animals ($n \geq 15$ per genotype) were monitored every 3 h after peritonitis induction over 72 h. During this experiment, animals received volume resuscitation (balanced saline solution) of 25 μ l/g BW twice per day subcutaneously over the period of the survival study. Log-rank statistics were used for data analysis.

Bacterial burden in blood and organs

Blood and organs were collected from deeply anesthetized WT and KO mice ($n \geq 4$ per genotype per time point) 6 h after PCI. Sodium citrate was used as an anticoagulant. After blood was harvested, whole liver and lungs were collected in a sterile manner. To avoid bacterial contamination, collected organs were briefly washed in 70% ethanol. The organs were later homogenized in sterile 0.9% saline solution. Enriched brain-heart infusion (2 ml) was added to each sample, and dilutions up to five orders of magnitude were prepared. These dilutions were plated on Schädler's and blood agars and incubated under aerobic and anaerobic conditions for 48 h. The number of bacterial colonies was counted. Data were evaluated with consideration of blood volume or normalized to wet weight of organs.

Blood analysis

Whole blood was collected by heart puncture from sham-treated and septic animals ($n \geq 15$ per genotype per time point) 6 h after peritonitis induction. Leukocyte and platelet counts were determined for aSMase WT and KO animals using the automated veterinary hematology analyzer Poch-100iv-Diff (Sysmex, Leipzig, Germany).

Leukocyte subpopulations were also analyzed in whole blood collected from both genotypes. Blood smears were prepared and stained using Giemsa. The slides were then processed for analysis using the automated analyzer Cellavision DM 96 (Sysmex, Leipzig, Germany).

Serum was collected from aSMase WT and KO animals at three time points ($n \geq 8$ per genotype per time point) for analysis of laboratory markers of organ dysfunction using the clinical chemistry analyzer Fuji Dri-Chem 3500i (Sysmex, Leipzig, Germany) according to the manufacturer's instructions.

Measurement of phagocytotic activity

Phagocytotic activity of granulocytes and monocytes was determined by flow cytometry after incubating whole blood samples with FITC-labeled and opsonized *Escherichia coli* (Phagotest; Becton Dickinson, Franklin Lakes, NJ). Briefly, 6 h after PCI, blood was collected from sham and septic WT and KO animals ($n \geq 4$ per genotype per time point) using Li-heparin as an anticoagulant. Diluted blood was incubated with labeled *E. coli* (1.7×10^9 /ml) for 20 min at 37°C followed by washing, lysis, and staining. The samples were measured by flow cytometry according to the manufacturer's instructions (software: CellQuest Pro, version 5.1.1). After "gating" FITC-positive monocytes and granulocytes, groups were compared with each other.

Quantification of cytokines in plasma

Cytokines (IL-6, IL-10, monocyte chemoattractant protein [MCP]-1, and TNF- α) were quantified in EDTA plasma samples collected from sham and septic WT and KO animals at three time points ($n \geq 6$ per genotype per time point) using cytometric bead assay (Becton Dickinson) according to the manufacturer's instructions.

Granulocyte-migration studies

Livers were collected from WT and KO animals ($n = \geq 4$ per genotype per time point) at three time points. Transmigration of leukocytes into liver tissue was evaluated by specific staining of granulocytes in liver sections. These sections (3 μm) were deparaffinized with decreasing ethanol series. The LEUCOGNOST[®] NASDCL kit (Merck Millipore, Darmstadt, Germany) was used for staining transmigrated granulocytes following the user's manual. At 400 \times magnification, stained cells were counted in at least 20 visual fields by two independent and experienced scientists blinded to treatment or genotype.

Intravital microscopy

In vivo imaging of the liver was performed with an epifluorescence microscope as described in detail previously (26) to evaluate leukocyte endothelium interactions 6 h after insult in sham-treated and in septic aSMase WT and KO animals ($n = 5$ per genotype per time point). Leukocytes were labeled in vivo with carboxyfluorescein diacetate succinimidyl ester (1 mg/kg BW) administered via a central line 10 min before surgical instrumentation. At least five regions of interest per mouse of either postsinusoidal venules (40 \times objective lens) or sinusoids (10 \times objective lens) were recorded over 30 s and 5 s, respectively (GFP filterset, 470–495 nm excitation and 525–550 nm emission band pass filters). Leukocytes were considered as “rollers” when they rolled across the endothelium or stuck to the endothelium for a few seconds and then detached. Leukocytes were considered as “stickers” when they remained stuck to the endothelium throughout the observation period. The total number of leukocytes in the postsinusoidal venules was calculated per mm^2 endothelial surface (length of observed vessel segment \times diameter $\times \pi$). Rollers and stickers in postsinusoidal venules were calculated per 100 counted leukocytes. Stickers in sinusoids as well as transmigrated leukocytes were calculated per mm^2 liver surface (27).

Protein expression on leukocytes

Expression of surface proteins CD49d, CD62L, and CD11b was analyzed using flow cytometry according to the manufacturer's instructions (software: CellQuest Pro, version 5.1.1). Briefly, whole blood was collected from aSMase WT and KO animals ($n = 9$ per genotype per time point). Samples of whole blood were separately incubated with FITC-labeled CD49d, CD62L, and CD11b antibodies. The geo-mean of fluorescence intensity (MFI) of all gated leukocytes was documented.

Determination of ceramide content in circulating leukocytes

Whole blood was collected from aSMase WT and KO animals at baseline and 6 h after sepsis induction ($n = \geq 12$ per genotype per time point). The ceramide pattern was fixed by the addition of an unspecific, broad-spectrum inhibitor of hydrolases (diisopropyl fluorophosphate) during the lysis of red blood cells. Washed and pelleted leukocytes were pooled (to obtain 1–2 million cells per sample; six samples per group) and resuspended in methanol. After addition of 20 pmol C17-ceramide, chloroform, methanol, and distilled water to the cells followed by intense vortexing and centrifugation, the lower organic phase was obtained for further analysis. Lipids were then resolved in methanol after evaporation of the organic phase via the SpeedVac SC201 ARC vacuum system (Thermo Fisher Scientific GmbH, Dreieich, Germany).

Analysis was performed using a quadrupole/time-of-flight mass spectrometer (Agilent, Waldbronn, Germany) connected to a rapid-resolution liquid chromatograph. High-purity nitrogen for the mass spectrometer was produced by a nitrogen generator (Parker Balston, Maidstone, UK).

Chromatographic separations were obtained using a ZORBAX Eclipse XDB-C18 as described previously (Agilent Technologies, Waldbronn, Germany) (28). The injection volume per sample was 10 μl . Best results were obtained with an isocratic elution (acetonitrile/2-propanol 3:2 with 1% formic acid) at a flow rate of 1 ml/min for 15 min. For mass spectrometric measurements, we used the following ion source conditions and gas settings for positive LC-MS/MS: sheath gas temperature: 400°C, sheath gas flow: 9 l/min, nebulizer pressure = 30 psig, drying gas temperature = 350°C, drying gas flow = 8 l/min, capillary voltage = 2,000 V, fragmentor voltage = 355 V, nozzle voltage = 2,000 V. All ceramides gave the same fragment ion of m/z 264.27 at different retention times depending on their chain length. Quantification was performed using Mass Hunter software (Agilent). Calibration curves of reference ceramide values were performed from 1 to 100 pmol and were constructed by linear fitting using the least squares linear regression calculation. The resulting slope of the calibration curve was used for calculating the concentration of the respective analyte in the unknowns.

Measurement of aSMase activity in plasma

Citrated plasma was collected from aSMase WT and KO animals ($n = \geq 6$ per genotype per time point) 6 h after the insult. aSMase activity was determined by the hydrolysis of fluorescently labeled sphingomyelin (NBD-SM; Molecular Probes, Eugene, OR) as a substrate, chromatographic product separation, and image analysis as described previously (15, 29). Plasma samples were diluted 1:10 with the incubation buffer (sodium acetate, pH 5.0) before analysis. The final composition of the reaction mixture was 12 μl plasma, and the extraction was carried out using the SpeedVac concentrator Plus (Eppendorf, Hamburg, Germany).

Determination of reactive oxygen species formation in circulating granulocytes

Whole blood was collected from aSMase WT and KO animals at baseline and 6 h after sepsis induction ($n = 6$ per genotype per time point). Granulocytes were labeled with a PE-labeled Ly-6G antibody (eBioscience Inc., San Diego, CA). For the detection of reactive oxygen species (ROS), we used the FagoFlowEx kit according to the manufacturer's instructions (EXBIO, Vestec, Czech Republic). Briefly, blood samples were incubated with *E. coli* and dihydrorhodamine-123. After red blood cell lysis, the resuspended leukocytes were analyzed for detection of ROS formation using flow cytometry according to the manufacturer's instructions (software: CellQuest Pro, version 5.1.1). The fluorescence signal was expressed as MFI. We measured MFI for sham samples and those incubated with *E. coli*. Results are represented as a stimulation index, which was calculated by normalization of the *E. coli* mix against the control.

Gene expression analysis and qPCR

Whole blood and tissue samples (liver and lung) were collected from aSMase KO mice and their WT littermates 6 and 24 h after sepsis ($n = 2$ per genotype per time point). Organs were shock frozen for later isolation of total RNA. Samples were analyzed by a pangenomic microarray mouseWG-6 v1.1 expression bead chips using an iScan platform (Illumina, San Diego, CA) measuring the variation of expression rate of >42,000 transcripts. Subsequent to biostatistical analysis, validation of expression data of representative genes was performed by quantitative real-time PCR. Data were normalized to unchanged reference transcripts (*Actb*, *Gapdh*, *Hprt*), and relative changes were plotted against sham-treated WT littermates.

Statistics

Data were obtained from randomly selected animals for each time point. Analyses were generally performed in an independent

setting with respect to the measure. Thus, each animal reflects a discrete set of data. For ethical reasons, when possible and appropriate different tissues, organs, and whole blood samples from one animal were used for several measurements (i.e., samples for determination of leukocyte counts, leukocyte subpopulations, and platelet counts in whole blood were obtained from the same animals). The same applied for the analyses of bacterial burden from blood and organs and granulocyte migration studies. All data were examined for normal distribution, and appropriate tests were applied. Statistical differences between groups were analyzed using ANOVA followed by Student-Newman-Keuls post hoc test or ANOVA (Kruskal-Wallis test) followed by pairwise multiple comparison procedures (Dunn's method) or Mann-Whitney rank-sum test. Data are given as boxplots, which show the median and the first and third quartiles and whiskers (10th and 90th percentiles). *P* values below 0.05 were considered statistically significant.

RESULTS

Discriminating values of ceramide content in circulating leukocytes highlighted the differences between the two genotypes. Despite the loss of sphingomyelinase, cell-bound ceramide was found significantly increased at baseline in KO animals compared with the WT littermates. Reflecting the biological significance of ceramide generation, levels of ceramide in leukocytes significantly increased only in WT animals 6 h after the septic insult (Fig. 1).

For characterization of the bacterial load, solid organs and blood samples collected from WT and KO mice were investigated for their content of aerobic and anaerobic bacteria. The two genotypes exhibited differences in bacterial load subsequent to sepsis. In KO animals, the number of colony-forming units (CFUs) of aerobes and anaerobes in liver as well as the aerobes in blood were significantly higher compared with WT animals. Blood anaerobes were similarly high in both WT and KO groups. Surprisingly, the number of CFU in lungs of KO was lower

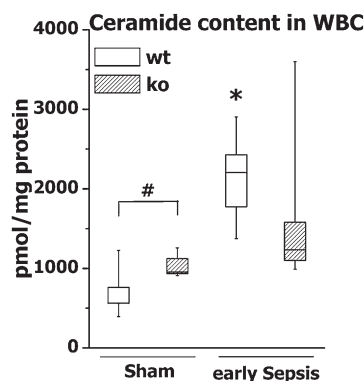


Fig. 1. Ceramide accumulation in circulating leukocytes. Blood was collected from aSMase WT and KO animals at baseline and 6 h after sepsis induction ($n = \geq 12$ per genotype per time point). Data were obtained from six samples per genotype. Each sample contained 1 to 2 million cells pooled from WT or KO animals. Therefore, solely in this figure, animal to animal deviations are not shown. Measurements were normalized to protein content. * $P < 0.05$ versus sham; # $P < 0.05$ between genotypes. WBC, white blood cells.

compared with WT animals. CFUs of anaerobes did not significantly increase in the KO animals 6 h after sepsis induction (Fig. 2). As a negative control, vehicle-treated control mice (sham) exhibited no CFU in blood or in liver and lung.

The levels of proinflammatory mediators reflect important markers of disease progression and are linked to the activation status of the innate immune system. After PCI, cytokine levels increased over time (baseline, 6 h, and 24 h) independent of the genotype (Fig. 3). In WT and KO animals, 6 h after sepsis induction, cytokine levels of IL-6 and MCP significantly increased in both genotypes. However, we measured a significantly higher increase in the levels of the prototypical anti- and proinflammatory cytokines TNF- α and IL-10 in KO animals 6 h after sepsis induction compared with WT animals. At 24 h, a further increase in cytokine levels of TNF- α and MCP could be observed in KO animals compared with WT littermates without reaching significance.

To evaluate the distinct cytokine profiles as a cause or consequence of sphingomyelinase activity and ceramide formation, we further investigated the inflammatory response in a systems biology approach using a tissue-specific transcriptomal analysis. Across all tissues (circulating leukocytes, liver, and lung), more than 26,000 transcripts were found expressed. After normalization and hierarchical clustering analysis, only seven annotated transcripts exhibited a different expression compared with untreated animals of each genotype (e.g., *Gpnmb*, *Hexa*, *CD83*). In aSMase KO animals with peritonitis, transcripts were found differentially regulated when compared with WT littermates at both time points ($n = 258$ at 6 h; $n = 315$ at 24 h) (Fig. 4A). The transcripts for *Tnfa*, *Nfkb1a*, *Casp4*, *Ccl4*, *Ccl7*, *Mapkaph2*, *Csf3*, *Stat3*, and *Il1rn* were found to be differentially regulated (supplementary Table I). These transcripts included those crucially involved in inflammation, immune regulation, and inflammatory response against invading pathogens. qPCR confirmed a sharp increase of selected transcripts relevant to regulation of inflammatory response, such as cytokines and cytokine-regulated transcripts (e.g., *Tnf*, *Tnfaip3*) in KO animals (Fig. 4B).

The data obtained from the quantification of bacterial burden, cytokine profiling, and transcriptome analysis urged us to further determine the total count of monocytes and their ability to phagocytize circulating pathogens. Although WT and KO groups revealed a significant decrease in monocyte counts 6 h after the septic insult (Fig. 5A), phagocytotic activity significantly increased in both genotypes. However, in KO animals, there was a significantly higher increase in phagocytotic activity compared with WT littermates (Fig. 5B). In contrast, no changes in absolute counts or phagocytotic activity of granulocytes were detected (data not shown).

Characterizing the distinct phenotypes upon sepsis induction, we established parameters of host response, such as complete blood and platelet counts. In whole blood, leukocyte and platelet counts were significantly reduced in both WT and KO groups 6 h after sepsis induction (Fig. 5C, D). Only minor changes in leukocyte subpopulations

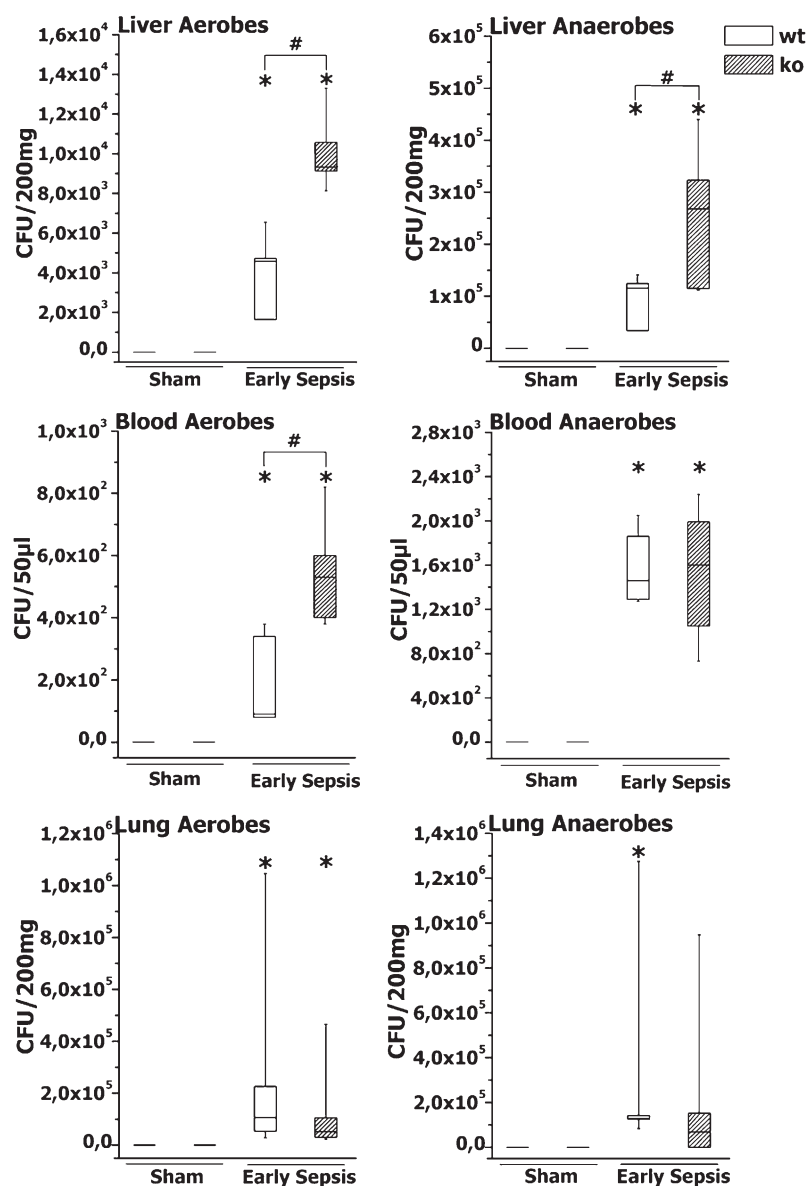


Fig. 2. Bacterial load in blood, liver, and lung depicted as CFUs. Blood and organs were collected 6 h after the septic insult from WT and KO animals ($n \geq 4$ per genotype per time point). Liver and blood cultures showed more elevated CFU counts in KO animals compared with WT animals. Lower CFUs were isolated from the lungs of KO animals. In sham mice, no microorganisms were registered. * $P < 0.05$ versus sham; # $P < 0.05$ between genotypes.

were observed in the WT group (Fig. 5E). However, KO animals revealed significant changes in the leukocyte subpopulations with a drop in lymphocyte and monocyte counts and a subsequent increase in the number of neutrophils (Fig. 5F).

Based on the differences in leukocyte subpopulation profiles between the genotypes, we were interested in the fate of leukocytes during sepsis. For this purpose, leukocyte-endothelial interaction in postsinusoidal venules and sinusoids were analyzed by intravital microscopy. The number of leukocytes significantly decreased in both groups 6 h after the septic insult, which is in line with the quantification of leukocytes in whole blood (Fig. 6A). However, there was a difference in the leukocyte-endothelial interaction between the genotypes highlighted by differences in rolling and attachment. The number of rollers (per 100 counted leukocytes) increased significantly 6 h after PCI from 6.26 to 11.45% in WT animals. However, there was no increase in the number of rollers in the KO group (Fig. 6B). The representative image demonstrates

the change in leukocyte counts in both genotypes and the increase in the number of rollers only in the WT animals (Fig. 6C). Similarly, the number of stickers in liver sinusoids significantly increased in the WT animals from 38 to 66 sticking leukocytes per mm² liver surface 6 h after the septic insult. No significant changes were observed in the KO group (Fig. 6D, E).

Analysis of leukocyte-endothelium interaction suggests that leukocytes are transmigrating from the circulation into the tissue. To confirm this process, we estimated the number of granulocytes transmigrated into liver parenchyma by cell-specific immunohistochemical staining. Both genotypes revealed a significant increase in the number of transmigrated granulocytes 6 h after the septic insult. However, these values significantly dropped in both genotypes 24 h after the septic insult (Fig. 7A).

To explain the differences in leukocyte rolling and sticking between the genotypes, we characterized the activation status of the cells. For this purpose, we monitored the expression of surface proteins relevant for rolling and sticking

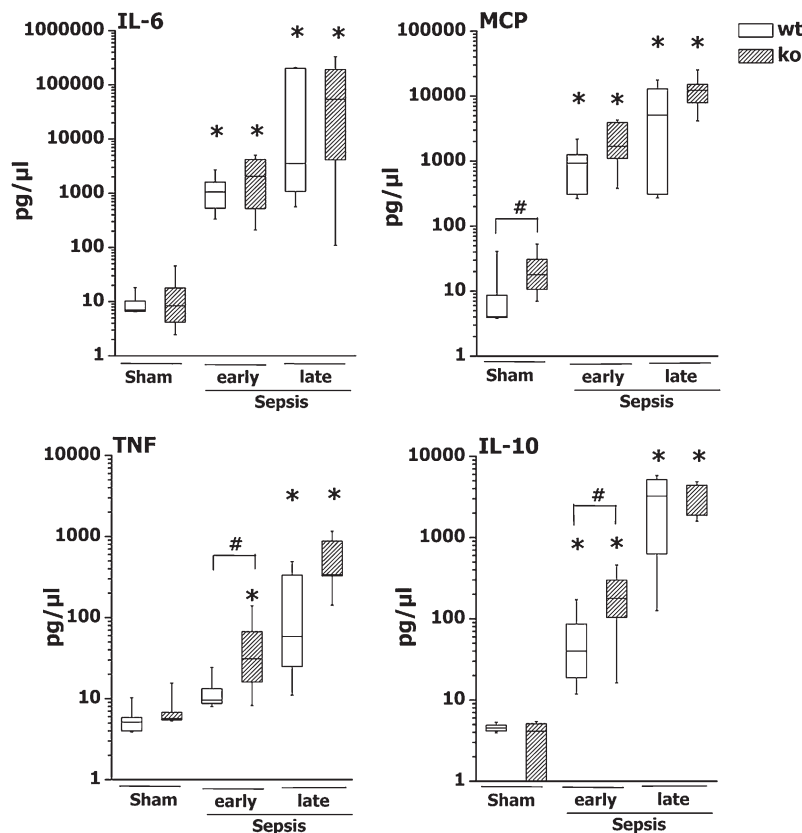


Fig. 3. Cytokine profiling during sepsis in aSMase WT and KO animals ($n \geq 6$ per genotype per time point). Plasma levels of cytokines increased during the progress of host response in both genotypes. KO animals show a more pronounced increase in cytokine levels 6 and 24 h after sepsis. * $P < 0.05$ versus sham; # $P < 0.05$ between genotypes. IL-6, interleukin-6; IL-10, interleukin-10; MCP-1, monocyte chemotactic protein-1; TNF- α , tumor necrosis factor α .

functions. Six hours after sepsis induction, the expression of CD49d was significantly down-regulated in KO animals. There was no change in the expression of CD49d in WT animals over time (Fig. 7B). A slight numerical increase in the expression of CD62L was only observed in WT animals 6 h after the septic insult without reaching significance (Fig. 7C). The expression of CD11b was significantly up-regulated only in WT animals 6 h after sepsis (Fig. 7D).

When determining the release of ROS from circulating leukocytes as a measure of the activated phenotype, we found a significant 2-fold increase 6 h after sepsis induction in both genotypes compared with baseline (sham-treated animals). No significant differences were monitored with respect to aSMase deficiency (Fig. 7E).

The development of organ dysfunction is a major consequence of transmigration of activated leukocytes into the tissue. Therefore, we measured established markers of hepatic and renal dysfunction or injury during the course of our sepsis model. At baseline, there were no differences between the genotypes in liver markers of cholestasis and hepato-cellular injury (aspartate transaminase [AST], alanine transaminase [ALT], gamma glutamyl-transferase [GGT], and total bilirubin [T-Bil]). Six hours after the septic insult, there were changes in the markers of hepatocellular injury where AST and ALT were significantly increased only in KO animals but dropped 18 h after the septic insult. There was a significant increase in levels of T-Bil in WT and KO animals in the late phase. The levels of T-Bil were slightly more increased in KO animals compared with WT animals without reaching significance. No changes in the levels of GGT were observed in WT and KO animals 6 and 18 h after sepsis (Fig. 8A).

Measurement of kidney function markers BUN and creatinine revealed differences between the two genotypes in sham-treated and septic animals. After the septic insult, BUN levels increased in WT and KO groups, reaching significance only in the KO animals. The levels of BUN continued to significantly increase at 18 h in both genotypes and more so in KO animals, reaching significance. Levels of creatinine were significantly higher in KO animals at the baseline and 6 h time points compared with WT littermates. These levels significantly increased in both genotypes 18 h after the septic insult. This increase was more pronounced in the KO animals, reaching significance (Fig. 8B).

Our model of abdominal cavity infection was found to be effective with respect to triggering severe infection and host response (25). With the absence of aSMase in the KO animals and the significant increase in the activity in WT littermates after sepsis (Fig. 9A), we expected to observe a higher survival rate in KO animals compared with the WT animals due to the limited ceramide generation. Surprisingly, aSMase WT and KO animals showed a similar pattern in mortality with an onset of mortality at 21 h and an end-survival of approximately 20% (Fig. 9B).

DISCUSSION

Here we characterize the role of aSMase in the early phase of host response to life-threatening infection. For this purpose, we used the model of PCI to obtain a severe polymicrobial sepsis that closely reflects the clinical situation as observed in around 50% of patients admitted to the

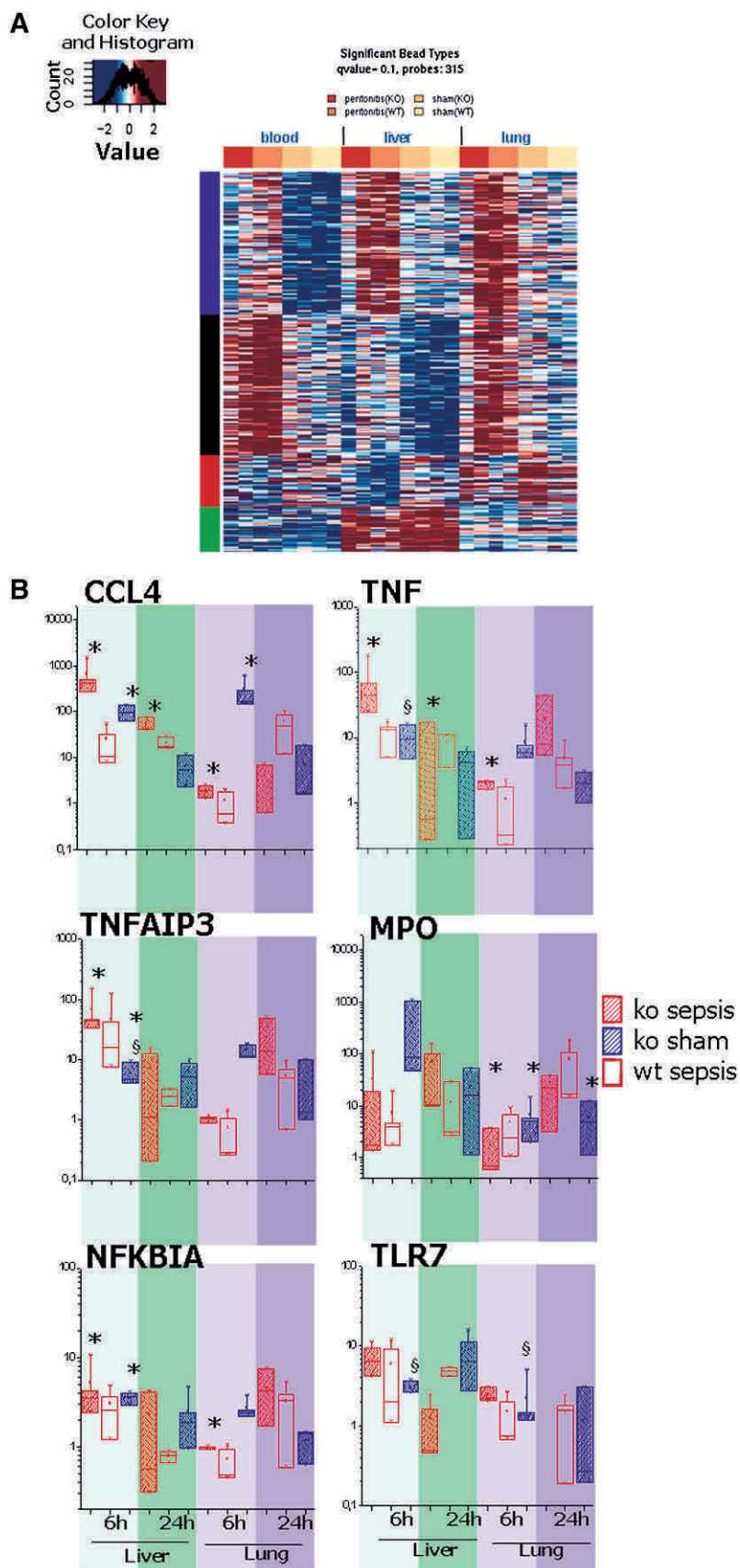


Fig. 4. A: Heatmap of differentially expressed transcripts. The expression patterns in circulating leukocytes and liver and lung tissues were analyzed after the collection of whole blood and organs 6 and 24 h after sepsis ($n = 2$ per genotype per time point) using the Illumina iScan microarray system. After normalization and statistical analysis, hierarchical cluster analysis was performed. Relative expression values are indicated by color code. In the columns, intervention and genotype are indicated by dark red for peritonitis in KO animals, light red for peritonitis in WT littermates, and dark orange and light orange for sham-treated KO and WT animals, respectively. B: qPCR data of selected genes normalized to WT sham group. $*P < 0.05$ versus WT sepsis; $§P < 0.05$ versus KO sepsis. CCL4, chemokine (C-C motif) ligand 4; MPO, myeloperoxidase; NFKBIA, nuclear factor of kappa light polypeptide gene enhancer in B-cells inhibitor α ; TLR7, Toll-like receptor 7; TNF, tumor necrosis factor; TNFAIP3, tumor necrosis factor α -induced protein 3.

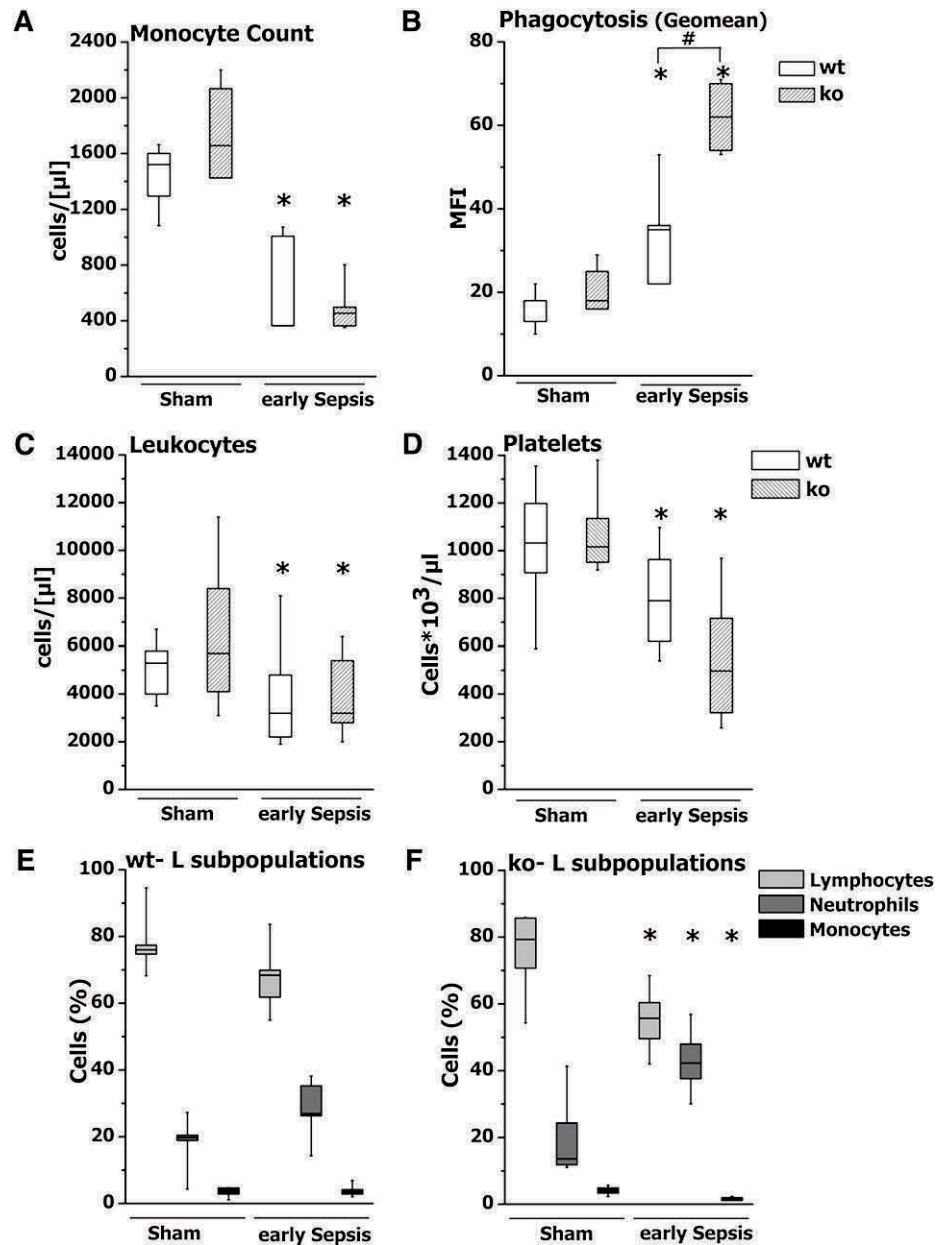


Fig. 5. Leukocyte phenotyping and platelet counts. A and B: Blood was collected from WT and KO animals 6 h after sepsis ($n \geq 4$ per genotype per time point). A: Monocyte counts decreased in both genotypes 6 h after sepsis. $*P < 0.05$ versus sham (B). Phagocytotic activity is depicted as mean fluorescent intensity (MFI). KO animals had a more elevated phagocytotic activity 6 h after sepsis compared with WT animals. $*P < 0.05$ versus sham; $\#P < 0.05$ between genotypes. C: Leukocytes ($n \geq 15$ per genotype per time point). Leukocytes significantly decreased in WT and KO animals 6 h after peritonitis. D: Platelets ($n \geq 15$ per genotype per time point). Platelets significantly dropped in WT and KO animals 6 h after peritonitis. $*P < 0.05$ versus sham. For leukocyte subpopulations, blood was collected from aSMase WT and KO animals 6 h after the insult. E: Minor changes in the subpopulations were observed in the WT group 6 h after the septic insult. F: Significant changes were observed in the KO animals. $*P < 0.05$ versus sham.

ICU due to sepsis, severe sepsis, and septic shock (30). This method involves the collection of stools from nonvegetarian donors followed by extensive microbiological characterization, preparation, and storage. This model reflects a reproducible and standardized, nontrauma method that results in a diffuse peritonitis similar to the clinical situation in cases such as perforated viscus due to diverticulitis. An acute onset of the disease is followed by systemic inflammation highlighted by an elevated bacterial burden as

well as a cytokine storm (27, 31–33). In the present study, the high bacterial burden in liver and blood and the rise in the levels of cytokines as well as parameters of organ dysfunction 6 h after the septic insult confirm an infectious focus and the development of severe sepsis.

With the development of sepsis, secreted aSMase activity is increased and breaks down inert cell membrane-embedded sphingomyelin into highly active ceramide, which accumulates, forming lipid rafts. It has been recently speculated

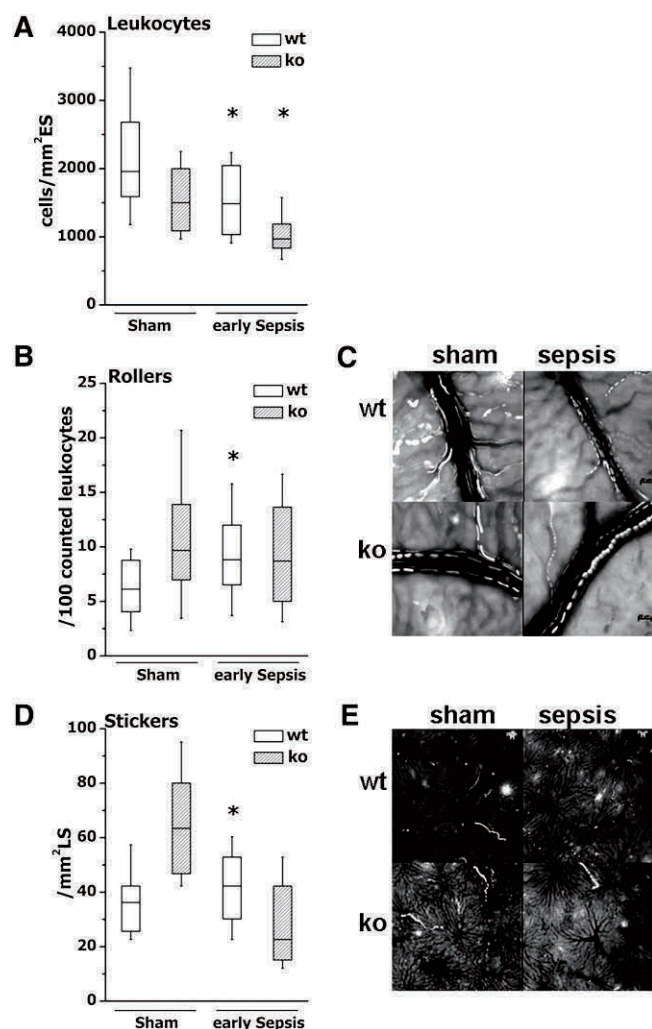


Fig. 6. Leukocyte counts in postsinusoidal venules and rolling and sticking in postsinusoidal venules and sinusoids as assessed by intravital microscopy 6 h after the septic insult ($n = 5$ per genotype per time point). **A:** Leukocyte counts in aSMase WT and KO animals. Indicated are the leukocyte counts per mm^2 endothelial surface (ES). $*P < 0.05$ versus sham. **B:** Leukocyte-endothelium interaction in aSMase WT and KO animals. Indicated are the rollers per 100 counted leukocytes. $*P < 0.05$ versus sham. **C:** Representative illustration of leukocyte-endothelium interaction in postsinusoidal venules of sham versus sepsis WT and KO animals. Depicted are overlays of all images of a 30 s video of postsinusoidal venules from sham-treated animals and those undergoing PCI. **D:** Sticking and transmigrated leukocytes in liver sinusoids of aSMase WT and KO animals. Indicated are the stickers per mm^2 liver surface (LS). $*P < 0.05$ versus sham. **E:** Representative illustration of leukocyte-endothelium interaction in sinusoids of a WT animal versus a KO animal. Depicted are overlay images of 5 s videos of a region in the sinusoids of sham-treated animals and those undergoing PCI (final magnification, 100 \times).

that in lipid storage diseases such as aSMase deficiency, immune cells may not obviate an appropriate inflammatory response (34).

To clarify a potential beneficial or maladaptive role of aSMase in the host response to sepsis, we compared data obtained from animals with a complete loss of function model to their WT littermates. The difference between the genotypes was elucidated in the measurement of ceramide

content in circulating leukocytes. Due to variation in the number of white blood cells analyzed, we normalized the ceramide values to protein content. In KO animals, levels of ceramide were significantly higher compared with WT littermates but did not increase after sepsis induction. These ceramide levels at baseline (as well as after sepsis induction), resulting from unknown compensatory mechanisms, are enough to maintain a normal function at a healthy state but not under septic conditions. The missing increase of ceramide in the KO animals after sepsis outlines the pivotal role of this enzyme in the rapid and transient formation of ceramide. Here we describe that the increase in the activity of aSMase (12) is reflected by a biological correlate. This increase might safeguard an appropriate cellular stress response but might also be, in an overwhelming fashion, a trigger of tissue damage (35). Without overinterpretation of our present data with the WT model, we could speculate that the increase in activity could be the cause or the consequence with respect to tissue damage and the development of organ failure. Although the increase in sphingomyelinase activity might originate from (active) release by stimulated (endothelial) cells (20) or passively from the lysosomes of damaged tissues, the biological activity in circulation per se might be interpreted as a hallmark of systemic stress response. There are several reports addressing the abundance of lysosomal proteins, such as chitinase or granulocytic elastase, during sepsis (36, 37). We also determined that the enzyme might be relevant for triggering cellular stress response in remote cells and tissues. During sepsis, the lack of lysosomal activity in transgenic mice might hinder an essential signaling pathway of cellular stress response, leading to macrophage activation and inflammation due to sphingomyelin accumulation (38). To perform best practice procedures and to avoid a potential bias caused by substrate accumulation, we enrolled in our experimental setting animals aged 8–10 weeks (24) where this phenotype is not yet developed. On the other hand, aSMase-deficient animals with cystic fibrosis appear to be more resistant to *Pseudomonas* infections with a decreased pulmonary inflammation. However, the absence of lysosomal aSMase could play a role, together with the more prominent course of infection, in the development of a more pronounced organ dysfunction observed in the present study (panel 8) as compared with WT littermates. Thus, the absence of lysosomal activity could possibly obviate benefits obtained through the decreased levels of secreted aSMase (8).

We expected a better outcome with the KO model when compared with WT littermates. The results instead highlighted a crucial role of aSMase in the early phase of host response to sepsis. The complete loss of function model resulted in a hyperresponsive state due to significantly higher bacterial burden mirrored by a more potent inflammatory response, thereby resulting in a similar outcome as compared with WT littermates through different trajectories.

The importance of aSMase during the early phase of sepsis was highlighted by the analysis of bacterial burden,

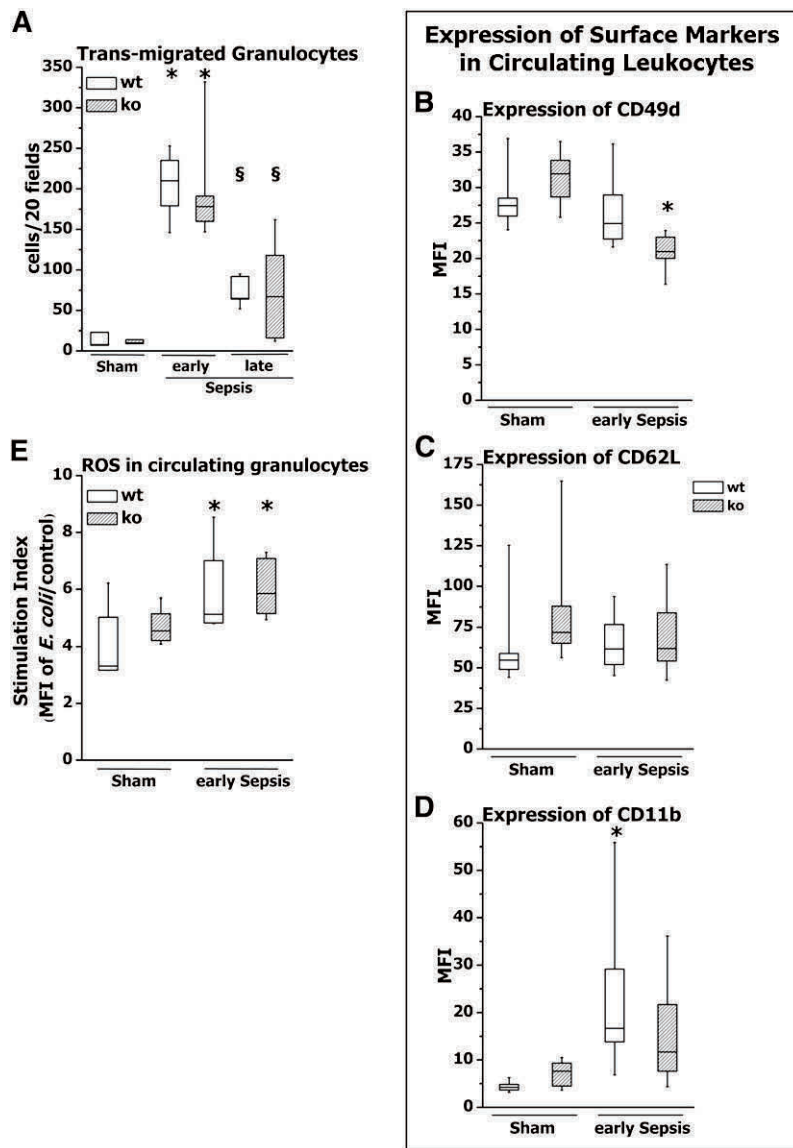


Fig. 7. A: Transmigration studies of granulocytes into liver tissue. Transmigration of granulocytes was determined by cell-specific immunohistochemical staining in aSMase WT and KO animals ($n \geq 4$ per genotype per time point). The number of migrated granulocytes in liver tissue increased in both WT and KO groups 6 h after the septic insult and decreased at 24 h after the insult. * $P < 0.05$ versus sham; § $P < 0.05$ versus 6 h sepsis. For the expression of surface markers on leukocytes, protein expression was assessed by flow cytometry in aSMase WT and KO animals ($n = 9$ per genotype per time point). B: CD49d expression was significantly down-regulated only in KO animals 6 h after sepsis. C: Minor changes in the expression of CD62L were observed in WT animals after PCI. D: Expression of CD11b was up-regulated only in WT animals 6 h after sepsis. * $P < 0.05$ versus sham. E: ROS formation in circulating granulocytes of aSMase WT and KO animals ($n = 6$ per genotype per time point). Intracellular ROS formation was significantly elevated after peritoneal infection. Values are presented as the stimulation index of MFI of *E. coli* exposed granulocytes versus MFI of untreated cells. * $P < 0.05$ versus sham. MFI, mean fluorescent intensity

which suggested a pivotal role of the enzyme in eliminating invading bacteria. Six hours after sepsis induction, bacterial burden of aerobes and anaerobes in the liver was significantly higher in KO animals compared with WT littermates. KO animals also registered a significantly higher CFU of aerobes in blood compared with WT animals. This suggests an inability of aSMase KO animals to efficiently eliminate microorganisms. Ceramide produced by activated aSMase plays a crucial role in innate immune response with respect to the elimination of microorganisms (39). Ching et al. (40) suggested that the absence of the enzyme left murine animals more susceptible to Sindbis virus-induced fatal encephalomyelitis. Unlike WT animals, aSMase KO mice were unable to eliminate *P. aeruginosa* from the lung upon acute pulmonary infection and died from sepsis a few days later (41). Without reaching significance, we registered a lower CFU in lungs of KO animals compared with WT littermates. This might be explained by the altered lung pathology in aSMase KO animals characterized by a significant increase in cell counts in the pulmonary spaces consisting mainly of enlarged and

multinucleated macrophages, which also registered an increased production of chemokines (38).

As key humoral mediators, we investigated the cytokine pattern in plasma. We noticed an earlier anti-inflammatory response in KO animals. Therefore, impairment of aSMase activation exhibited distinct effects on cytokine release. Moreover, kinetic and peak concentrations were in part different from the WT at the two observation time points in our study. This is an interesting observation because the pharmacological inhibition of aSMase has been characterized with a decreased transcription and secretion of TNF- α directly acting on relevant peripheral cell types in a polymicrobial sepsis model (42, 43). Also, in an in vitro model of cellular stress response triggered by prototypic electrophiles as triggers of cellular damage, aSMase activation resulted in an increase in the expression of TNF- α , amplifying generation of IL-6. Both knock-down and pharmacological inhibition abrogated cytokine response under these conditions (44), whereas the overexpression of aSMase, resulting in ceramide generation, induced TNF- α sensitivity measured by IL-6 secretion (44).

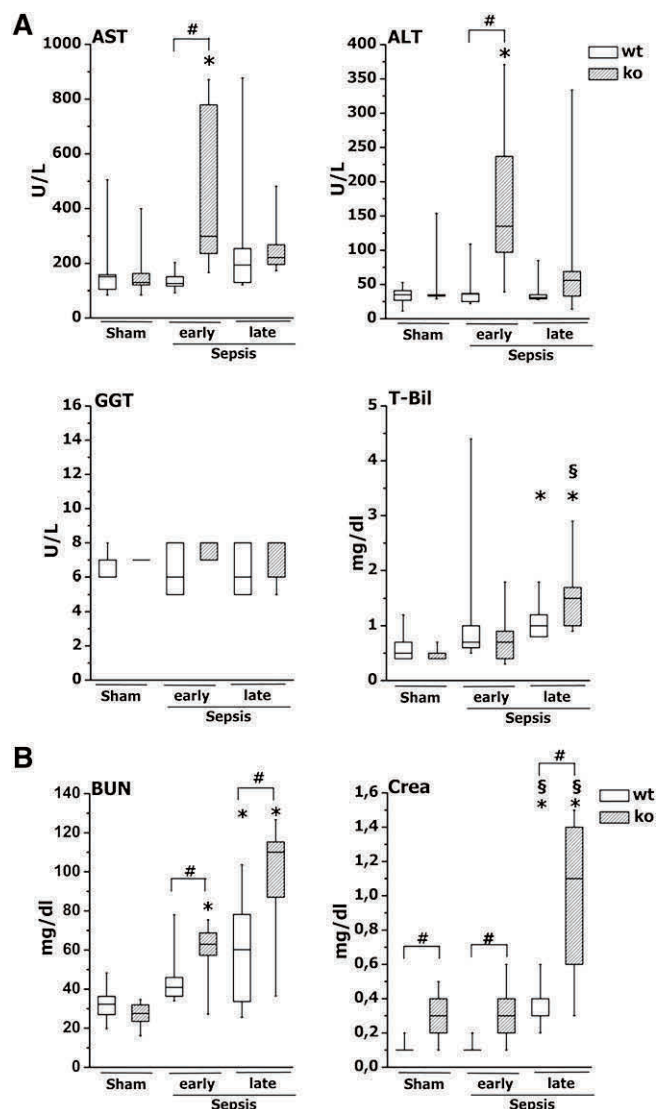


Fig. 8. Morbidity. Data were obtained at baseline and at 6 and 18 h after the septic insult ($n \geq 8$ per genotype per time point). A: Laboratory markers of liver dysfunction. * $P < 0.05$ versus sham; # $P < 0.05$ between genotypes; § $P < 0.05$ versus 6 h sepsis. AST, aspartate transaminase; ALT, alanine transaminase; GGT, gamma glutamyl-transferase; T-Bil, total bilirubin. B: Laboratory markers of kidney dysfunction. * $P < 0.05$ versus sham; # $P < 0.05$ between genotypes; § $P < 0.05$ versus 6 h sepsis. BUN, blood urea nitrogen; Crea, creatinine.

In circulating leukocytes, expression of transcripts encoding for cyto- and chemokines as well as their receptors was found up-regulated in both genotypes during the course of sepsis, corresponding to the results of cytokine measurements in the blood.

We compared the *Tnfa* transcript expression in an ex vivo LPS-triggered stimulation of expression and release of the cytokine (45) with systemic TNF levels and organ-specific expression in our model of polymicrobial infection. We found an unaffected expression in the lung homogenates 6 h after peritonitis, similar to unchanged expression of *Tnfa* in peritoneal macrophages (45). On the other hand, in the present study, we registered an up-regulated expression of *Tnfa* in whole tissue homogenates of the liver

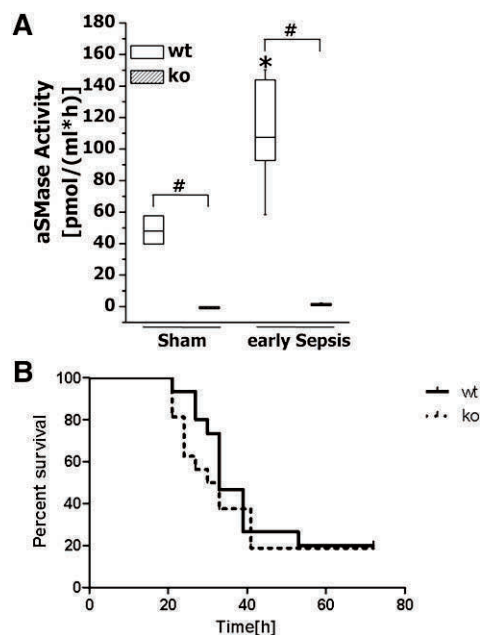


Fig. 9. aSMase activity and mortality. A: aSMase activity ($n \geq 6$ per genotype per time point). At baseline, aSMase activity was higher in WT animals compared with KO animals. After sepsis induction, aSMase activity significantly increased in WT animals. B: Survival analysis ($n \geq 15$ per genotype). Onset of mortality appeared at 21 h in both WT and KO groups. End survival was approximately 20% in both genotypes. * $P < 0.05$ versus sham; # $P < 0.05$ between the two groups.

6 h after sepsis induction, accompanied by higher systemic TNF- α levels. The hyper-responsive state in the KO animals revealed an overall higher bacterial burden in the liver compared with the lung. This more pronounced inflammatory response of the liver along with its pivotal role in host response in combination with higher organ mass, the exorbitant bacterial burden, and the cytokines levels in blood as well as the distinct role and response pattern of each organ during host response (46) enlighten the trajectory of the expression patterns in the different organs.

A panel of the relevant transcripts for immune regulation and bacterial elimination were differentially expressed in the lungs of aSMase-deficient animals compared with the WT littermates. Lysozyme and the astrocyte-elevated gene 1 (*Aeg1*, syn. *Mtdh*) were only found up-regulated in the lung tissue of aSMase-deficient animals (cluster 3). *Aeg1* is known as a TLR-4 specific regulator of NF- κ B-mediated cytokine synthesis (47). On the other hand, lysozyme (EC 3.2.1.17) is one of the most important secreted proteins hydrolyzing certain mucopolysaccharides of bacterial cell walls (48). Also functioning as primary regulators of ROS generation and essential components of the microbicidal oxidase system of phagocytes, both α and β subunits of the membrane-bound cytochrome b oxidase were found down-regulated in KO animals. These observations support the hypothesis that, beyond the altered lung physiology in KO animals, a genotype-specific regulation of transcripts involved in recognition and elimination of bacteria might have contributed to a better clearance of bacteria in the lungs.

Sepsis induced up-regulation of cathepsin G (*Ctsg*) was found diminished in aSMase-deficient mice. *Ctsg* is a serine protease participating in the killing and digestion of engulfed bacteria and regulates phagocytosis, degranulation, and ROS release (49, 50). The down-regulation of *Ctsg* in septic aSMase KO animals could therefore explain the inability of leukocytes to effectively eliminate phagocytised bacteria, which resulted in an overwhelming infection.

The dynamic, insult-specific variations of platelet and leukocyte counts were acknowledged as critical hints with respect to disease progression. Similar to the course in patients with sepsis, a significant drop in leukocyte and platelet counts was observed in both genotypes 6 h after sepsis induction. With the progression of systemic inflammation and infection, leukopenia and thrombocytopenia, which may function as indicators of disseminated intravascular coagulation, occur (50, 51). Further studies are needed to elucidate the proposed mechanism and to understand the role of aSMase in platelet activation and thrombocytopenia during sepsis.

The observation of leukopenia in WT and KO animals 6 h after sepsis induction raised the question of the fate of leukocytes during sepsis. This drop in cell count was confirmed with intravital microscopy of the liver where both genotypes exhibited a decrease in leukocytes in circulation after sepsis, which suggested the transmigration of the cells into the remote tissues. Indeed, 6 h after the septic insult, extravasation of leukocytes was reflected by a significant increase in transmigrated granulocytes into liver tissue in WT and KO animals. In patients with sepsis, the liver plays a principle role as a source of inflammatory mediators and acts as a remote organ for the effects of circulating inflammatory mediators released from other tissues. Transmigration of neutrophilic granulocytes can result from microcirculatory changes and leukocyte-endothelium interaction (52). The number and the activation status of transmigrated granulocytes are held responsible for the induction and retention of hepato-cellular dysfunction. Further analysis of the phenotype of transmigrated granulocytes could provide insight into the expression profile and the activation status of these leukocytes.

Speculating a distinct phenotype triggered by the enhanced cytokine storm and bacterial burden, we were able to detect this phenotype with a more elevated phagocytotic activity, a different leukocyte subpopulation profile, and a differentiated leukocyte expression pattern in KO animals compared with WT littermates. Phagocytotic activity increased significantly in both genotypes 6 h after the septic insult. However, this activity was more significantly increased in KO animals, reflected by a more elevated bacterial burden and higher levels of MCP in the blood. Although a more significant increase in phagocytotic activity was registered in KO mice, these animals still registered higher CFU values in blood and organs. This might suggest the inability of granulocytes to control intracellular microorganisms due to impairment in effector mechanisms. The lack of aSMase is not essential for the uptake of bacteria by the phagocytes but could play a crucial role in

their intracellular elimination (53). These results support our concept of the crucial role of aSMase in the early response to infection.

Although both genotypes registered a drop in total leukocyte counts 6 h after sepsis, we observed a different subpopulation profile in KO animals compared with WT animals. At baseline, both genotypes had similar subpopulation profiles. However, KO animals revealed a drop in lymphocytes and monocytes, mirrored by an increase in neutrophils 6 h after sepsis induction. With the development of sepsis, bacteria migrate into the tissue, inducing an inflammatory response. This includes the recruitment of neutrophilic granulocytes, as first line of defense, to the focus of infection and inflammation to combat invading microorganisms (54, 55). In the present study, KO animals have an overwhelming infection due to their inability to efficiently eliminate the microorganisms. This situation could explain the increased production of neutrophils in KO animals after sepsis as a combat strategy to overcome the overwhelming infection.

Another interesting finding was the differentiated leukocyte expression in KO animals compared with their WT littermates. Indeed, 6 h after sepsis induction, the expression of CD49d was significantly down-regulated in KO animals, whereas CD11b was significantly up-regulated only in WT animals. The missing increase in CD11b expression in KO animals might be due to their inability to produce ceramide and a subsequent lack of lipid raft formation necessary for CD11b recruitment (56).

This described phenotype might be one cause of a different course of the disease in the KO animals. The different leukocyte expression profile of CD49d and CD11b resulted in a different leukocyte-endothelium interaction between the two genotypes. CD49d, CD62L, and CD11b expression are essential for the rolling and sticking phenomenon leading to leukocyte-endothelium interaction (57, 58). In the present study, WT animals exhibited a significant increase in leukocyte rolling and sticking in the liver sinusoids and postsinusoidal venules 6 h after sepsis induction attributed to the up-regulation of expression markers on leukocytes. The down-regulation or missing increase in expression of these markers in the KO animals consequently resulted in an unchanged leukocyte-endothelium interaction between sham-treated and septic animals. Sepsis causes important changes in the liver, with alterations in hepatic macro- and microcirculation as well as leukocytes-endothelium interaction (59). The latter leads to neutrophil sequestration with subsequent local release of proinflammatory mediators and therefore plays a role in the development of liver dysfunction, which is a crucial event in the development of sepsis (27). It is unknown whether the phenotype of sequestered aSMase-deficient leukocytes have a rather beneficial or detrimental role with respect to development of organ dysfunction.

The proinflammatory cytokine TNF- α was found to be crucially involved in the generation of ROS (specifically H₂O₂) in a ceramide-dependent manner (60). The impotence in rapid ceramide generation in leukocytes of aSMase KO animals might be adjusted by the 2-fold

increase in circulating TNF levels to yield a similar ROS release in the two genotypes as observed here during sepsis. Thereby, with respect to the cytokine pattern, the earlier and more pronounced response might reflect a hyper-responsive status to overcome the inadequacy in ceramide-dependent pathways of host response.


The development of multiple organ injury is a major complication of sepsis and septic shock, increasing the lethality of sepsis to 70–80% (61, 62). To investigate the course of sepsis in remote organs, which were primarily affected during the continuum of the disease, different laboratory markers of organ dysfunction were measured. Dysfunction of the liver is considered a crucial complication in the course of human sepsis, is often limiting for prognosis (63), and was reflected here by a pronounced increase in markers of hepatocellular injury (AST and ALT) in KO animals in the early phase and in the marker of cholestasis (T-Bil) in the late phase of sepsis. Markers of hepatocellular injury dropped in the later phase of sepsis in KO animals, with an increase in the marker of cholestasis. In WT animals, markers of cholestasis and hepatocellular injury continued to rise in the later phase. A paradoxical up-regulation of a key determinant of transactivation of hepatic stellate cells was associated with the genetic ablation of aSMase, which was not restricted to the liver (64).

Similarly, acute renal failure is a common complication of critical illness. Levels of creatinine drastically increased (more so in KO animals) in the later phase of the disease. However, at baseline creatinine levels in KO animals were significantly higher compared with their WT littermates. This suggests that our aSMase KO animals are prone to kidney preinjury (65, 66).

The role of aSMase in diseases such as diabetes, cystic fibrosis, and chronic heart failure has been highly characterized in recent years (8, 16, 67). In the present study, we elucidated a crucial role of aSMase secretion through measurement of the stress-induced enzyme activity matched to accumulation of its product in circulating leukocytes in the early phase of sepsis. In a complete loss-of-function model, the pronounced amplitude of principle inflammation mediators such as cytokines and bacterial burden supported the concept that this enzyme is crucial in the first line defense against invading microorganisms. Loss of function resulted in a hyperresponsive state due to an overwhelming spread of microorganisms and the inability to effectively eliminate invading bacteria, leading to the generalization of host response.

The end result is highlighted in the survival analysis. Opposite to expectation, the complete loss-of-function model did not lead to a better survival. Instead, the overwhelming infection and inflammatory response led to a high mortality in KO similar to WT animals, which overall highlights the pivotal role of aSMase in sepsis.

In patients with sepsis, the increase of aSMase might function as an adaptive response mechanism. In our translational model we provided further insight into this process. It is evident that the conservation of this enzyme is crucial during the early phase through elimination of

invading microorganisms but could have detrimental effect during the late phase of sepsis. In line with this conclusion, stratification of patients pretreated with pharmacological inhibitors for other underlying conditions (i.e., major depression) might be of great value. In fact, a chronological inhibition of aSMase has been presenting a more favorable outcome in chronic infectious diseases such as cystic fibrosis with striking differences to the KO model (67). These results and the data from the present study encourage further research using a pharmacological-inhibition model as well as clinical studies with inhibitors of aSMase in patients with well-defined sepsis. 

The authors thank Bernhard Hube (HKI, Jena) for helpful comments and critical discussion and Wiebke Iffert for biostatistical analysis of the GWA.

REFERENCES

1. Martin, G. S., D. M. Mannino, S. Eaton, and M. Moss. 2003. The epidemiology of sepsis in the United States from 1979 through 2000. *N. Engl. J. Med.* **348**: 1546–1554.
2. Levy, M. M., R. P. Dellinger, S. R. Townsend, W. T. Linde-Zwirble, J. C. Marshall, J. Bion, C. Schorr, A. Artigas, G. Ramsay, R. Beale, et al. 2010. The Surviving Sepsis Campaign: results of an international guideline-based performance improvement program targeting severe sepsis. *Intensive Care Med.* **36**: 222–231.
3. Levy, M. M., A. Artigas, G. S. Phillips, A. Rhodes, R. Beale, T. Osborn, J. L. Vincent, S. Townsend, S. Lemeshow, and R. P. Dellinger. 2012. Outcomes of the Surviving Sepsis Campaign in intensive care units in the USA and Europe: a prospective cohort study. *Lancet Infect. Dis.* **12**: 919–924.
4. Hannun, Y. A., and L. M. Obeid. 2002. The Ceramide-centric universe of lipid-mediated cell regulation: stress encounters of the lipid kind. *J. Biol. Chem.* **277**: 25847–25850.
5. van Blitterswijk, W. J., A. H. van der Luit, R. J. Veldman, M. Verheij, and J. Borst. 2003. Ceramide: second messenger or modulator of membrane structure and dynamics? *Biochem. J.* **369**: 199–211.
6. Gulbins, E., and P. L. Li. 2006. Physiological and pathophysiological aspects of ceramide. *Am. J. Physiol. Regul. Integr. Comp. Physiol.* **290**: R11–R26.
7. Jenkins, R. W., D. Canals, and Y. A. Hannun. 2009. Roles and regulation of secretory and lysosomal acid sphingomyelinase. *Cell. Signal.* **21**: 836–846.
8. Smith, E. L., and E. H. Schuchman. 2008. The unexpected role of acid sphingomyelinase in cell death and the pathophysiology of common diseases. *FASEB J.* **22**: 3419–3431.
9. Gulbins, E. 2003. Regulation of death receptor signaling and apoptosis by ceramide. *Pharmacol. Res.* **47**: 393–399.
10. Goggel, R., S. Winoto-Morbach, G. Vielhaber, Y. Imai, K. Lindner, L. Brade, H. Brade, S. Ehlers, A. S. Slutsky, S. Schutze, et al. 2004. PAF-mediated pulmonary edema: a new role for acid sphingomyelinase and ceramide. *Nat. Med.* **10**: 155–160.
11. Goni, F. M., and A. Alonso. 2002. Sphingomyelinases: enzymology and membrane activity. *FEBS Lett.* **531**: 38–46.
12. Claus, R. A., M. J. Dorer, A. C. Bunck, and H. P. Deigner. 2009. Inhibition of sphingomyelin hydrolysis: targeting the lipid mediator ceramide as a key regulator of cellular fate. *Curr. Med. Chem.* **16**: 1978–2000.
13. Marathe, S., G. Kuriakose, K. J. Williams, and I. Tabas. 1999. Sphingomyelinase, an enzyme implicated in atherogenesis, is present in atherosclerotic lesions and binds to specific components of the subendothelial extracellular matrix. *Arterioscler. Thromb. Vasc. Biol.* **19**: 2648–2658.
14. Marathe, S., S. L. Schissel, M. J. Yellin, N. Beatini, R. Mintzer, K. J. Williams, and I. Tabas. 1998. Human vascular endothelial cells are a rich and regulatable source of secretory sphingomyelinase. Implications for early atherogenesis and ceramide-mediated cell signaling. *J. Biol. Chem.* **273**: 4081–4088.

15. Claus, R. A., A. C. Bunck, C. L. Bockmeyer, F. M. Brunkhorst, W. Losche, R. Kinscherf, and H. P. Deigner. 2005. Role of increased sphingomyelinase activity in apoptosis and organ failure of patients with severe sepsis. *FASEB J.* **19**: 1719–1721.
16. Doehner, W., A. C. Bunck, M. Rauchhaus, S. von Haehling, F. M. Brunkhorst, M. Ciccoira, C. Tschope, P. Ponikowski, R. A. Claus, and S. D. Anker. 2007. Secretory sphingomyelinase is upregulated in chronic heart failure: a second messenger system of immune activation relates to body composition, muscular functional capacity, and peripheral blood flow. *Eur. Heart J.* **28**: 821–828.
17. Drobniak, W., G. Liebsch, F. X. Audebert, D. Frohlich, T. Gluck, P. Vogel, G. Rothe, and G. Schmitz. 2003. Plasma ceramide and lysophosphatidylcholine inversely correlate with mortality in sepsis patients. *J. Lipid Res.* **44**: 754–761.
18. Delogu, G., G. Famularo, F. Amati, L. Signore, A. Antonucci, V. Trinchieri, L. Di Marzio, and M. G. Cifone. 1999. Ceramide concentrations in septic patients: a possible marker of multiple organ dysfunction syndrome. *Crit. Care Med.* **27**: 2413–2417.
19. Wong, M. L., B. Xie, N. Beatini, P. Phu, S. Marathe, A. Johns, P. W. Gold, E. Hirsch, K. J. Williams, J. Licinio, et al. 2000. Acute systemic inflammation up-regulates secretory sphingomyelinase in vivo: a possible link between inflammatory cytokines and atherogenesis. *Proc. Natl. Acad. Sci. USA.* **97**: 8681–8686.
20. Jenkins, R. W., D. Canals, J. Idkowiak-Baldys, F. Simbari, P. Roddy, D. M. Perry, K. Kitatani, C. Luberto, and Y. A. Hannun. 2010. Regulated secretion of acid sphingomyelinase: implications for selectivity of ceramide formation. *J. Biol. Chem.* **285**: 35706–35718.
21. Nikolova-Karakashian, M. N., and K. A. Rozenova. 2010. Ceramide in stress response. *Adv. Exp. Med. Biol.* **688**: 86–108.
22. Zhang, A. Y., F. Yi, G. Zhang, E. Gulbins, and P. L. Li. 2006. Lipid raft clustering and redox signaling platform formation in coronary arterial endothelial cells. *Hypertension.* **47**: 74–80.
23. Zhang, D. X., F. X. Yi, A. P. Zou, and P. L. Li. 2002. Role of ceramide in TNF- α -induced impairment of endothelium-dependent vasorelaxation in coronary arteries. *Am. J. Physiol. Heart Circ. Physiol.* **283**: H1785–H1794.
24. Horinouchi, K., S. Erlich, D. P. Perl, K. Ferlinz, C. L. Bisgaier, K. Sandhoff, R. J. Desnick, C. L. Stewart, and E. H. Schuchman. 1995. Acid sphingomyelinase deficient mice: a model of types A and B Niemann-Pick disease. *Nat. Genet.* **10**: 288–293.
25. Gonnert, F. A., E. Kunisch, M. Gajda, S. Lambeck, M. Weber, R. A. Claus, M. Bauer, and R. W. Kinne. 2012. Hepatic Fibrosis in a Long-term Murine Model of Sepsis. *Shock.* **37**: 399–407.
26. Recknagel, P., R. A. Claus, U. Neugebauer, M. Bauer, and F. A. Gonnert. 2012. In vivo imaging of hepatic excretory function in the rat by fluorescence microscopy. *J. Biophotonics.* **5**: 571–581.
27. Gonnert, F. A., P. Recknagel, M. Seidel, N. Jbeily, K. Dahlke, C. L. Bockmeyer, J. Winning, W. Losche, R. A. Claus, and M. Bauer. 2011. Characteristics of clinical sepsis reflected in a reliable and reproducible rodent sepsis model. *J. Surg. Res.* **170**: e123–e134.
28. Luth, A., C. Neuber, and B. Kleuser. 2012. Novel methods for the quantification of (2E)-hexadecenal by liquid chromatography with detection by either ESI QTOF tandem mass spectrometry or fluorescence measurement. *Anal. Chim. Acta.* **722**: 70–79.
29. Loidl, A., R. Claus, H. P. Deigner, and A. Hermetter. 2002. High-precision fluorescence assay for sphingomyelinase activity of isolated enzymes and cell lysates. *J. Lipid Res.* **43**: 815–823.
30. Levinson, A. T., B. P. Casserly, and M. M. Levy. 2011. Reducing mortality in severe sepsis and septic shock. *Semin. Respir. Crit. Care Med.* **32**: 195–205.
31. Rudiger, A., A. Dyson, K. Felsmann, J. E. Carre, V. Taylor, S. Hughes, I. Clatworthy, A. Protti, D. Pellerin, J. Lemm, R. A. Claus, M. Bauer, and M. Singer. 2012. Early functional and transcriptomic changes in the myocardium predict outcome in a long-term rat model of sepsis. *Clin Sci (Lond)* **124**: 391–401.
32. Lambeck, S., M. Weber, F. A. Gonnert, R. Mrowka, and M. Bauer. 2012. Comparison of sepsis-induced transcriptomic changes in a murine model to clinical blood samples identifies common response patterns. *Front Microbiol.* **3**: 284.
33. Recknagel, P., F. A. Gonnert, E. Halilbasic, M. Gajda, N. Jbeily, A. Lupp, I. Rubio, R. A. Claus, A. Kortgen, M. Trauner, et al. 2013. Mechanisms and functional consequences of liver failure substantially differ between endotoxaemia and faecal peritonitis in rats. *Liver Int.*
34. Lopez, M. E., A. D. Klein, J. Hong, U. J. Dimbil, and M. P. Scott. 2012. Neuronal and epithelial cell rescue resolves chronic systemic inflammation in the lipid storage disorder Niemann-Pick C. *Hum. Mol. Genet.* **21**: 2946–2960.
35. Haimovitz-Friedman, A., C. Cordon-Cardo, S. Bayoumy, M. Garzotto, M. McLoughlin, R. Gallily, C. K. Edwards 3rd, E. H. Schuchman, Z. Fuks, and R. Kolesnick. 1997. Lipopolysaccharide induces disseminated endothelial apoptosis requiring ceramide generation. *J. Exp. Med.* **186**: 1831–1841.
36. Duswald, K. H., M. Jochum, W. Schramm, and H. Fritz. 1985. Released granulocytic elastase: an indicator of pathobiochemical alterations in septicemia after abdominal surgery. *Surgery.* **98**: 892–899.
37. Maddens, B., B. Ghesquiere, R. Vanholder, D. Demon, J. Vanmassenhove, K. Gevaert, and E. Meyer. 2012. Chitinase-like proteins are candidate biomarkers for sepsis-induced acute kidney injury. *Mol Cell Proteomics* **11**: M111 013094.
38. Dhami, R., X. He, R. E. Gordon, and E. H. Schuchman. 2001. Analysis of the lung pathology and alveolar macrophage function in the acid sphingomyelinase-deficient mouse model of Niemann-Pick disease. *Lab. Invest.* **81**: 987–999.
39. Yu, H., Y. H. Zeidan, B. X. Wu, R. W. Jenkins, T. R. Flotte, Y. A. Hannun, and I. Virella-Lowell. 2009. Defective acid sphingomyelinase pathway with *Pseudomonas aeruginosa* infection in cystic fibrosis. *Am. J. Respir. Cell Mol. Biol.* **41**: 367–375.
40. Ng, C. G., and D. E. Griffin. 2006. Acid sphingomyelinase deficiency increases susceptibility to fatal alphavirus encephalomyelitis. *J. Virol.* **80**: 10989–10999.
41. Grassme, H., V. Jendrossek, A. Riehle, G. von Kurthy, J. Berger, H. Schwarz, M. Weller, R. Kolesnick, and E. Gulbins. 2003. Host defense against *Pseudomonas aeruginosa* requires ceramide-rich membrane rafts. *Nat. Med.* **9**: 322–330.
42. Roumestan, C., A. Michel, F. Bichon, K. Portet, M. Detoc, C. Henriquet, D. Jaffuel, and M. Mathieu. 2007. Anti-inflammatory properties of desipramine and fluoxetine. *Respir. Res.* **8**: 35.
43. Kornhuber, J., P. Tripal, M. Reichel, C. Muhle, C. Rhein, M. Muehlbacher, T. W. Groemer, and E. Gulbins. 2010. Functional Inhibitors of Acid Sphingomyelinase (FIASMs): a novel pharmacological group of drugs with broad clinical applications. *Cell. Physiol. Biochem.* **26**: 9–20.
44. Kumagai, T., T. Ishino, and Y. Nakagawa. 2012. Acidic sphingomyelinase induced by electrophiles promotes proinflammatory cytokine production in human bladder carcinoma ECV-304 cells. *Arch. Biochem. Biophys.* **519**: 8–16.
45. Rozenova, K. A., G. M. Deevska, A. A. Karakashian, and M. N. Nikolova-Karakashian. 2010. Studies on the role of acid sphingomyelinase and ceramide in the regulation of tumor necrosis factor α (TNF α)-converting enzyme activity and TNF α secretion in macrophages. *J. Biol. Chem.* **285**: 21103–21113.
46. Weber, M., S. Lambeck, N. Ding, S. Henken, M. Kohl, H. P. Deigner, D. P. Enot, E. I. Igwe, L. Frappart, M. Kiehnopf, et al. 2012. Hepatic induction of cholesterol biosynthesis reflects a remote adaptive response to pneumococcal pneumonia. *FASEB J.* **26**: 2424–2436.
47. Khuda, I. I., N. Koide, A. S. Noman, J. Dagvadorj, G. Tumurkhuu, Y. Naiki, T. Komatsu, T. Yoshida, and T. Yokochi. 2009. Astrocyte elevated gene-1 (AEG-1) is induced by lipopolysaccharide as toll-like receptor 4 (TLR4) ligand and regulates TLR4 signalling. *Immunology.* **128**: e700–e706.
48. Fleming, A. 1922. On a remarkable bacteriolytic element found in tissues and secretions. *Proc. R. Soc. Lond.* **93**: 306–317.
49. Reeves, E. P., H. Lu, H. L. Jacobs, C. G. Messina, S. Bolsover, G. Gabella, E. O. Potma, A. Warley, J. Roes, and A. W. Segal. 2002. Killing activity of neutrophils is mediated through activation of proteases by K⁺ flux. *Nature.* **416**: 291–297.
50. Dhainaut, J. F., S. B. Yan, D. E. Joyce, V. Pettita, B. Basson, J. T. Brandt, D. P. Sundin, and M. Levi. 2004. Treatment effects of drotrecogin α (activated) in patients with severe sepsis with or without overt disseminated intravascular coagulation. *J. Thromb. Haemost.* **2**: 1924–1933.
51. Saugel, B., A. Umgele, F. Martin, V. Phillip, R. M. Schmid, and W. Huber. 2010. Systemic Capillary Leak Syndrome associated with hypovolemic shock and compartment syndrome. Use of transpulmonary thermodilution technique for volume management. *Scand J Trauma Resusc Emerg Med.* **18**: 38.
52. Szabo, G., L. Romics, Jr., and G. Frendl. 2002. Liver in sepsis and systemic inflammatory response syndrome. *Clin. Liver Dis.* **6**: 1045–1066 (x).
53. Utermohlen, O., U. Karow, J. Lohler, and M. Kronke. 2003. Severe impairment in early host defense against *Listeria monocytogenes* in mice deficient in acid sphingomyelinase. *J. Immunol.* **170**: 2621–2628.

54. Fox, S., A. E. Leitch, R. Duffin, C. Haslett, and A. G. Rossi. 2010. Neutrophil apoptosis: relevance to the innate immune response and inflammatory disease. *J. Innate Immun.* **2**: 216–227.
55. Craciun, F. L., E. R. Schuller, and D. G. Remick. 2010. Early enhanced local neutrophil recruitment in peritonitis-induced sepsis improves bacterial clearance and survival. *J. Immunol.* **185**: 6930–6938.
56. Cao, C., Y. Gao, Y. Li, T. M. Antalis, F. J. Castellino, and L. Zhang. 2010. The efficacy of activated protein C in murine endotoxemia is dependent on integrin CD11b. *J. Clin. Invest.* **120**: 1971–1980.
57. Dadfar, E., J. Lundahl, E. Fernvik, A. Nopp, B. Hylander, and S. H. Jacobson. 2004. Leukocyte CD11b and CD62l expression in response to interstitial inflammation in CAPD patients. *Perit. Dial. Int.* **24**: 28–36.
58. Nuckel, H., M. Switala, C. H. Collins, L. Sellmann, H. Grosse-Wilde, U. Duhrsen, and V. Rebmann. 2009. High CD49d protein and mRNA expression predicts poor outcome in chronic lymphocytic leukemia. *Clin. Immunol.* **131**: 472–480.
59. Spapen, H. 2008. Liver perfusion in sepsis, septic shock, and multiorgan failure. *Anat. Rec. (Hoboken)*. **291**: 714–720.
60. Wang, L., H. Zhen, W. Yao, F. Bian, F. Zhou, X. Mao, P. Yao, and S. Jin. 2011. Lipid raft-dependent activation of dual oxidase 1/H₂O₂/NF-kappaB pathway in bronchial epithelial cells. *Am. J. Physiol. Cell Physiol.* **301**: C171–C180.
61. Bauer, M., F. Brunkhorst, T. Welte, H. Gerlach, and K. Reinhart. 2006. [Sepsis. Update on pathophysiology, diagnostics and therapy] [in German]. *Anaesthesist.* **55**: 835–845.
62. Brun-Buisson, C., F. Doyon, J. Carlet, P. Dellamonica, F. Gouin, A. Lepoutre, J. C. Mercier, G. Offenstadt, and B. Régnier. 1995. Incidence, risk factors, and outcome of severe sepsis and septic shock in adults. A multicenter prospective study in intensive care units. *JAMA.* **274**: 968–974.
63. Kortgen, A., M. Paxian, M. Werth, P. Recknagel, F. Rauchfuss, A. Lupp, C. G. Krenn, D. Muller, R. A. Claus, K. Reinhart, et al. 2009. Prospective assessment of hepatic function and mechanisms of dysfunction in the critically ill. *Shock.* **32**: 358–365.
64. Moles, A., N. Tarrats, J. C. Fernandez-Checa, and M. Mari. 2012. Cathepsin B overexpression due to acid sphingomyelinase ablation promotes liver fibrosis in Niemann-Pick disease. *J. Biol. Chem.* **287**: 1178–1188.
65. Kuemmel, T. A., J. Thiele, R. Schroeder, and W. Stoffel. 1997. Pathology of visceral organs and bone marrow in an acid sphingomyelinase deficient knock-out mouse line, mimicking human Niemann-Pick disease type A. A light and electron microscopic study. *Pathol. Res. Pract.* **193**: 663–671.
66. Philit, J. B., G. Queffeuilou, F. Walker, M. C. Gubler, E. Dupuis, F. Vrtovsniak, and F. Mignon. 2002. Membranoproliferative glomerulonephritis type II and Niemann-Pick disease type C. *Nephrol. Dial. Transplant.* **17**: 1829–1831.
67. Becker, K. A., H. Grassme, Y. Zhang, and E. Gulbins. 2010. Ceramide in *Pseudomonas aeruginosa* infections and cystic fibrosis. *Cell. Physiol. Biochem.* **26**: 57–66.